electronics

MDPI

Article

Mid-Infrared Emission in $Ge/Ge_{1-x}Sn_x/Ge$ Quantum Well Modeled Within 14-Band *k.p* Model

Omar Zitouni [1,2], Nouha Mastour [1] and Said Ridene [1,*]

[1] Advanced Materials and Quantum Phenomena Laboratory, Physics Department, Faculty of Sciences of Tunis, University of Tunis El Manar, Tunis 2092, Tunisia; ozitouni555@gmail.com (O.Z.); mastournouha@yahoo.fr (N.M.)
[2] El Manar Preparatory Engineering Institute—IPEIEM, University of Tunis El Manar, Tunis 2092, Tunisia
* Correspondence: said.ridene@fst.rnu.tn

Abstract: Band structure and gain in a $Ge/Ge_{1-x}Sn_x/Ge$ quantum well are described theoretically using a 14-band *k.p* model. It has been shown that the quantum well width and the α-Sn concentration considerably modify the conduction and valence subband structure, and, as a result, the optical gain changes with the insertion of a very small concentration of α-Sn. In particular, we have determined the necessary injection carrier density *Nj* and the critical α-Sn concentration for elevated high gain lasing. It is found that for $Nj = 1.5 \times 10^{18}$ cm^{-3}, we achieved a maximum peak gain for α-Sn concentration of the order 0.155. We can predict that $Ge/Ge_{1-x}Sn_x/Ge$ QWs should be manufactured with an α-Sn concentration less than 0.155 in devices for optoelectronics applications such as telecommunication and light emitting laser diodes.

Keywords: $Ge/Ge_{1-x}Sn_x/Ge$ QW; 14-band *k.p* theory; critical α-Sn concentration; mid-infrared emission

check for updates

Citation: Zitouni, O.; Mastour, N.; Ridene, S. Mid-Infrared Emission in $Ge/Ge_{1-x}Sn_x/Ge$ Quantum Well Modeled Within 14-Band *k.p* Model. *Electronics* **2024**, *13*, 4142. https://doi.org/10.3390/electronics13214142

Academic Editors: Martino Aldrigo, Ana-Maria Lepadatu, Florin Nastase and Andrei Avram

Received: 8 July 2024
Revised: 18 August 2024
Accepted: 20 August 2024
Published: 22 October 2024

Copyright: © 2024 by the authors. Licensee MDPI, Basel, Switzerland. This article is an open access article distributed under the terms and conditions of the Creative Commons Attribution (CC BY) license (https://creativecommons.org/licenses/by/4.0/).

1. Introduction

Ge, Sn group-IV-materials have drawn a remarkable amount of interest for both their electronic and optical properties [1–4]. The optical properties, such as laser and optical gain, can be enhanced when the Ge semiconductor is combined with the semi-metallic α-Sn. Recently, SiGeSn quantum well (QW) structures have shown enormous benefits in both theoretical and experimental studies [5–10]. However, significant progress in optoelectronic devices, such as infrared photodetectors in terahertz wavelength regions, has been reported by using GeSn/SiGeSn [11] or by optimization of different structural parameters of SiGeSn [12]. In addition, the optoelectronics properties of SiGeSn are greatly enhanced by the optimization of the α-Sn concentration, in particular by the transition from an indirect to direct band gap [13,14]. However, it is experimentally shown that the direct bandgap structure can be acquired by the incorporation of a small concentration of α-Sn [8], and that a high photoluminescence intensity can be also attained. Indeed, the elaboration and photoluminescence characterization of GeSn has significantly contributed to the growth of Si-based optoelectronics technology [9,13]. Further, several practical investigations demonstrated that the direct bandgap structure of $Ge_{1-x}Sn_x$ can be obtained with $x = 0.12$ [15]. In addition, thanks to changing the bandgap of GeSn, the ternary alloy SiGeSn also presents an analogous inter-band transition. Furthermore, several experimental and theoretical studies demonstrated that the ternary alloy SiGeSn has a higher range of bandgap and lattice variation compared with the binary one, therefore providing supplementary applications. An interesting question is related to the threshold carrier densities of GeSn QW laser light emission and the physical cause of low-temperature lasing of current. This has been studied in order to evaluate the threshold carrier densities of habitual III–V and II-VI QW lasers [16]. Indeed, the lasing has been investigated, and it has been shown that optical gain emission behavior analogous to II–VI and III–V QW has been found for GeSn QW by

n-type doping of 6×10^{18} cm^{-3}. In addition, a theoretical analysis of GeSn quantum dots for photodetection applications has also been conducted [17].

Up to now, the optical properties performances such as the optical cross section and the optical gain emission of GeSn/Ge QW have been considered with 6- and 8-band ***k.p*** Hamiltonian. To investigate the optimal injection carrier density and concentration of α-Sn with Ge, it is essential to apply the 14-band model in order to consider the effect of the far conduction (CB) and valence bands (VB) levels, which can considerably influence the inter-band-transitions and optical gain emission procedure. Compared to the 8-band ***k.p*** model, the 14-band ***k.p*** Hamiltonian is more appropriate in applications involving a sensible injection carrier density and doped concentration. This can be explained by the far levels bands intervening in the 14-band *k.p* model, such as the [(Γ_{7C}, Γ_{8C})-Γ_{6C}, (Γ_{7C}, Γ_{8C})-(Γ_{7V}, Γ_{8V}) and Γ_{6C}-(Γ_{7V}, Γ_{8V})] interactions, which represent, respectively, the coupling between the two-type of CBs, the higher-CB with VB, and the coupling between the lower-CB and VB, whereas the 8-band *k.p* Hamiltonian is governed only by the lower-CB with VB interaction. Thus, in this paper, we theoretically consider the influence of the injection carrier density and the α-Sn concentration on the CB and VB-band structures and the wave functions as well as the optical gain emission through the framework of the 14-band ***k.p*** model, taking into account the strain effect and the interaction between VB and CB-bands. For the numerical step, we employ self-consistent iteration and variational methods [5,18].

2. Theoretical Method for Optical Laser-Gain of Ge/Ge$_{1-x}$Sn$_x$/Ge QWs

Investigations of optical gain properties, such as injection carrier density and α-Sn concentration, require accurate knowledge of the subband structure. However, both the CB and VB subbands of Ge/Ge$_{1-x}$Sn$_x$/Ge QW will be investigated by the 14-band ***k.p*** Hamiltonian H [5,18]:

$$H = H_{kp} + H_{strain} + V_{VBO}(z) + V_{CBO}(z) \quad (1)$$

where H_{kp} represent the ***k.p*** Hamiltonian, H_{strain} represents the Hamiltonian of strain, and $V_{VBO}(z)$ and $V_{CBO}(z)$ are, respectively, the VB and CB potential offset. The bands alignment scheme and CB and VB parameters used in 14-band ***k.p*** model of the Ge/Ge$_{1-x}$Sn$_x$/Ge QWs are represented in Figure 1. The H_{kp}, matrix, and the $|J, M_J\rangle$ base are given in Appendix A.

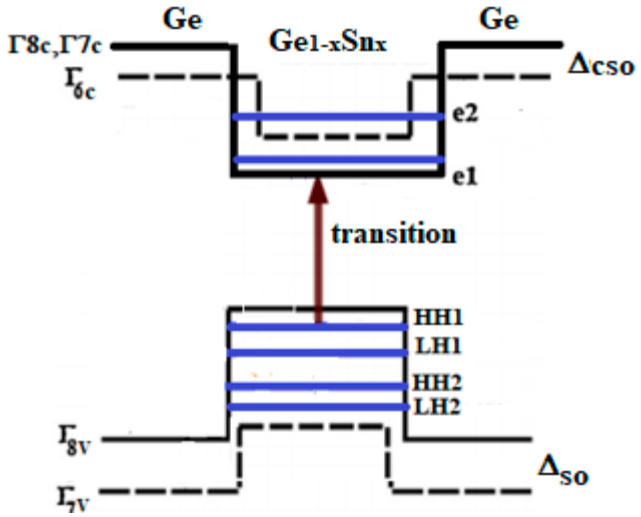


Figure 1. Bands alignment structure of Ge/Ge$_{1-x}$Sn$_x$/Ge QWs. Δ_{SO} and Δ_{CSO} represent the spin orbit splitting energies of the CB and VB, respectively.

For the optical gain $g(\omega)$ calculation, it is well known that $g(\omega)$ for QW depends on the subband structure and is related to the density of states ρ_{2D}, the wave functions overlap,

the intra-band relaxation time τ_{in}, the quasi-Fermi levels f_n^c and f_m^v, and on the momentum matrix element for the optical transitions [19]:

$$g(\omega) = \frac{e^2}{m_0^2 n_r\, c\, \varepsilon_0\, \omega} \frac{1}{L_{QW}} \sum_{\sigma=\uparrow,\downarrow} \sum_{n\ m} J_{cv}^{n\ m} \int_0^{+\infty} \rho_{2D} |M_{cv}|^2 \left[f\left(E_{n,k}^c - E_F^c\right) - f\left(E_F^v - E_{m,k}^v\right) \right] \times \frac{\hbar/\tau_{in}}{\left(\hbar\omega - (E_{n,k}^c - E_{m,k}^v) - E\right)^2 + (\hbar/\tau_{in})^2} dE \quad (2)$$

where, m_0 is free electron mass, L_{Qw} is well width, n_r is refractive index, e is the electron charge, ε_0 is the permittivity of free space, c is the light-velocity, and τ_{in} is the intraband relaxation time, which is equal to 10^{-13} s [19].

3. Results and Discussions

To study the effect of the QW-width and the α-Sn concentration on the subband structure and optical gain, we calculated the relation dispersion of both CB and VB of the $Ge/Ge_{1-x}Sn_x/Ge$ QW for α-Sn concentration and QW-width. The necessary parameters of Ge and α-Sn used in the present numerical calculation are given in Table 1 of reference [18]. The well and barrier width are around (8, 10, 12, 14) nm and 24 nm, respectively, and the profound for the well is about 130 meV for the heavy HHn and light LHn-holes [20]. Note that the unit of the energy is meV and the energy reference is chosen at the highest of the unstrained HHn-well. All the numerical parameters of the bulk Ge and α-Sn used in this work are taken from Refs. [18,20].

Figure 2 plots the subband structure of the CB and VB of a 12 nm single QW with various Sn concentration.

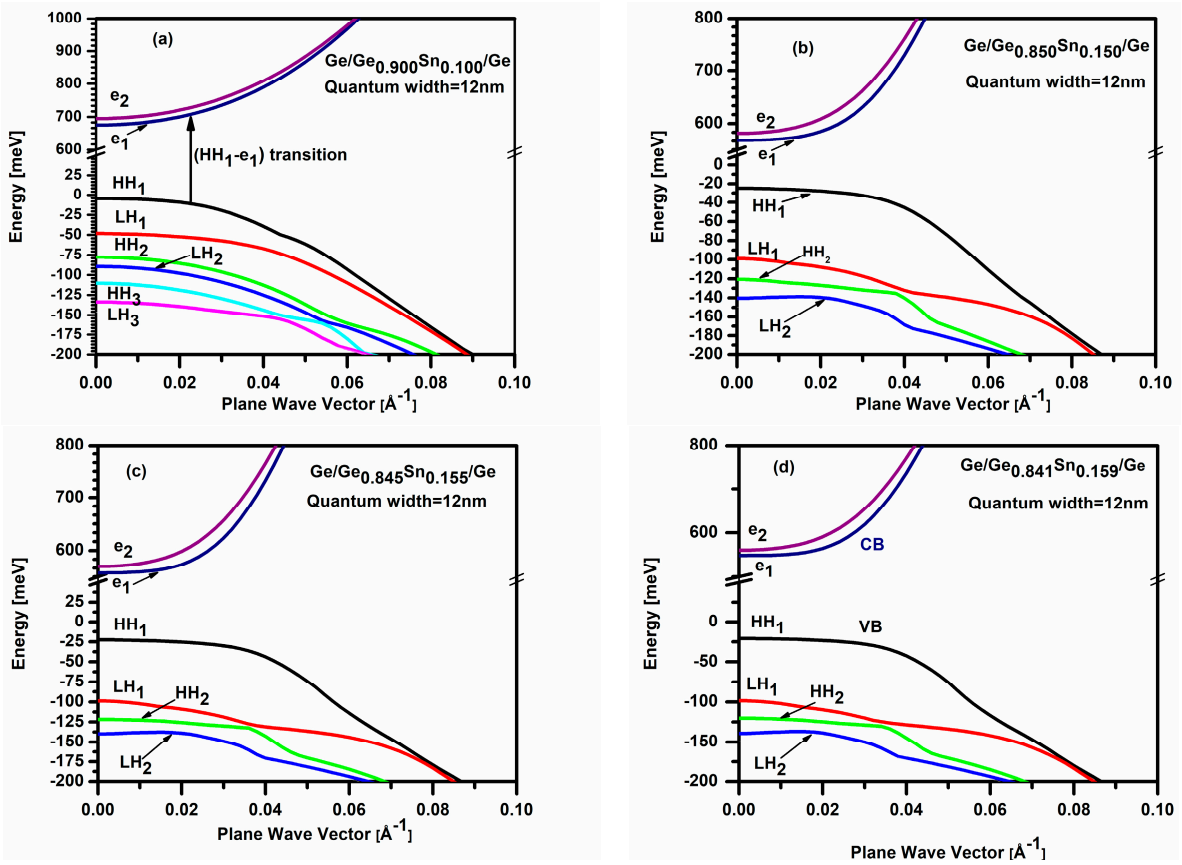


Figure 2. CB- and VB-subband structure of $Ge/Ge_{1-x}Sn_x/Ge$ QW calculated for α-Sn concentrations 0.1, 0.15, 0.155, and 0.59, respectively.

The HH_n, LHn, and e_n represent the confined hole- and electron-subband-states in CB and VB, respectively, for various α-Sn concentrations. For the different behaviors, one should note the strong non-parabolicities resulting from the admixture of (HHn, LHn) in the VB. Indeed, strong coupling has been shown between the HHn, and LHn. This reality suggests that the VB-states are highly dependent between them and with the two CBs in the $Ge/Ge_{1-x}Sn_x/Ge$ QW. One can notice that the number of confined states and the difference between the HHn and LHn subbands increase with α-Sn concentration. On the other hand, from Figure 2, we notice that both the HH_1- and HH_2-states are shifted down, whereas the LH_1-states are pressed up when the concentration of Sn increases. This can be attributed to the influence of α-Sn concentration on the band gap energy [11], which can explain the higher energy level as shown in Figure 2a. In addition, the HH_1-e_1-transition energy is very dependent on the α-Sn concentration, and it is shifted to the low-energies. This comportment will considerably influence the variation of the optical gain. Optical gain emission for different QW-width (8, 10, 12, and 14 nm) and α-Sn (0.1 0.15, 0.155, and 0.159) concentrations of the *$Ge/Ge_{1-x}Sn_x/Ge$ QW* are represented in Figure 3a–d.

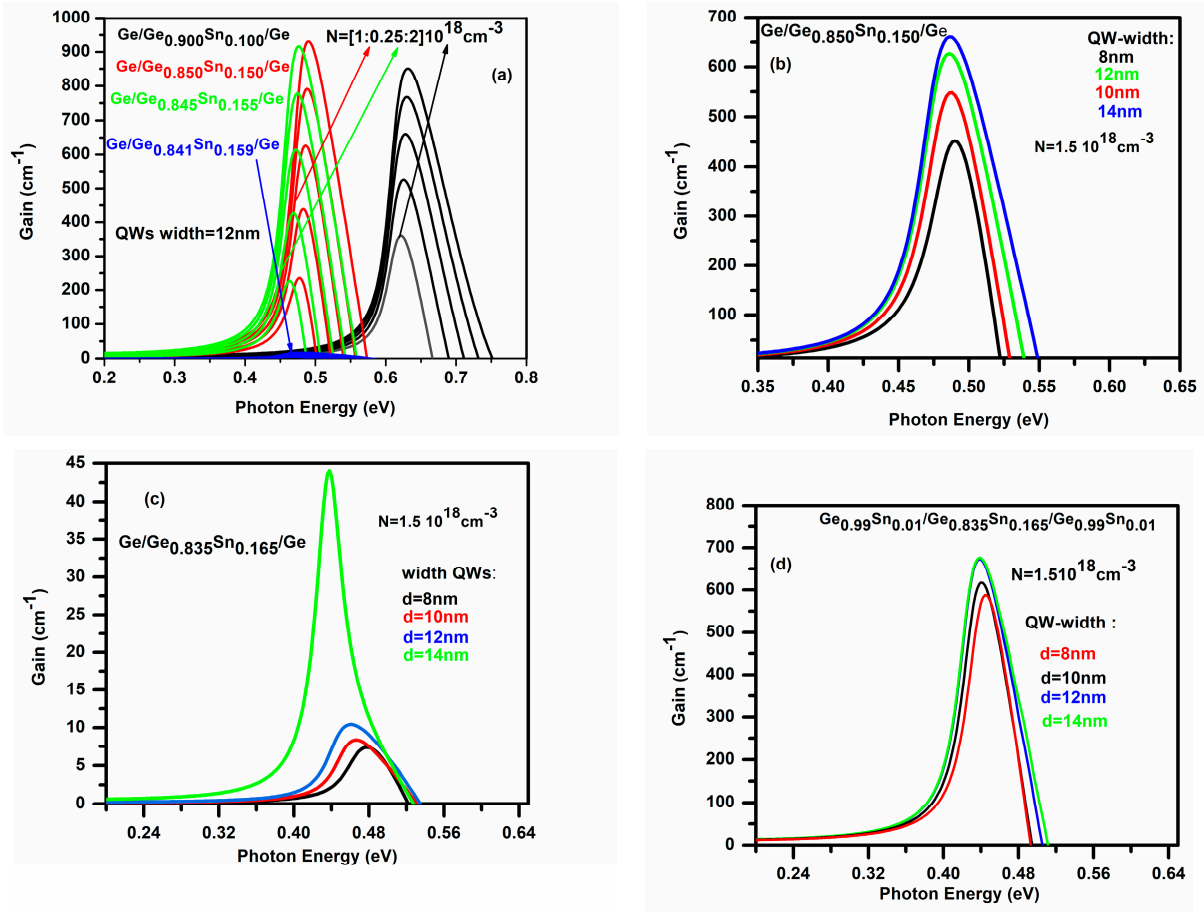


Figure 3. Optical gain versus photon energy in $Ge/Ge_{1-x}Sn_x/Ge$ QW calculated: (**a**) for different carrier injection densities *N* and different concentrations of α-Sn (0.1 0.15, 0.155, and 0.159). The red, green, and black arrows point to the increase in the different carrier injection densities *N* [1:0.25:2]10^{18} cm^{-3}. (**b**–**d**) are determined for typical injected carrier density (1.5×10^{18} cm^{-3}) and for different QW-width.

We notice that the optical gain curves are very sensitive to the α-Sn concentration and to the QW-width. The injected carrier density has been chosen to overcome the free carrier absorption losses [6] and it is varied from $N_j = 1 \times 10^{18}cm^{-3}$ to $2 \times 10^{18}cm^{-3}$. It is important to note that within the 8-band ***k.p*** Hamiltonian, the injected carrier density has been varied from $N_j = 2 \times 10^{18}cm^{-3}$ to $6 \times 10^{18}cm^{-3}$ in references [7,16]. One can observe

that for the value of *x* between 0.1 and 0.159, the gain peak moves to a higher wavelength when we increase the Sn concentration, i.e., we reached an emission wavelength of the order of 1.96 µm for x = 0.1, whereas for x = 0.155, an emission value in the order of 2.61 µm was obtained. These results confirm that mid-infrared laser structure operating at room temperature can be obtained by $Ge/Ge_{1-x}Sn_x/Ge$ QW structure. Otherwise, for x = 0.159, we remarked the strong reduction for optical gain. We reached an intensity lesser than 50 cm^{-1}, whereas for x = 0.155 an intensity in the order of 929 cm^{-1} has been obtained. Therefore, this variance does not exist in the calculations provided by the 8-band model [2,7]. Furthermore, the 14-band ***k.p*** Hamiltonian 0.155 represents the critical concentration of a-Sn, which leads to the strong decrease in the intensity of the optical gain as presented in Figure 4. In order to highlight the evolution of wavelength and the peak gain maximum versus α-Sn concentration, we plotted (in Figure 4) the wavelength extracted from the peak gain maximum as a function of the insertion of the α-Sn contents.

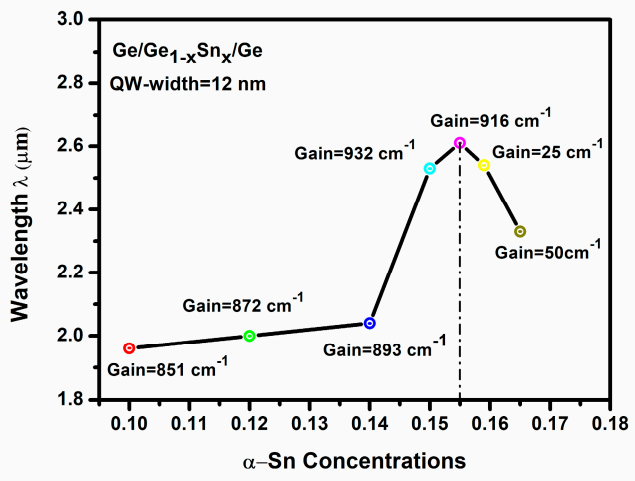


Figure 4. Wavelength in $Ge/Ge_{1-x}Sn_x/Ge$ QW as a function of the insertion of the α-Sn contents at the peak gain maximum values and for 12 nm QW-width.

It is observed that the increase of α-Sn concentration from 0.1 to 0.155 increases both the wavelength and the gain maximum. Beyond these concentrations, one can notice the strong decrease of optical gain and the wavelength. This indicates that 0.155 represents the critical α-Sn concentration for elevated high gain lasing for the $Ge/Ge_{1-x}Sn_x/Ge$ QW structure. By comparing the 8-band and 14-band models, the maximum injected carrier density used to produce gain is less than 2×10^{18} cm^{-3} for the 14-band model while it is greater than 6×10^{18} cm^{-3} for the 8-band model [2,7,16]. This difference in the injected carrier density justifies the importance of the application of the 14-band model for the GeSn structures. On the other hand, in refs [7,16], the authors indicate that the enlargement of the QW-width can considerably enhance the optical gain. Thus, we have reviewed the optical gain dependence on QW-width. Figure 3a displays the optical gain of $Ge/Ge_{1-x}Sn_x/Ge$ QW calculated for x = 0.150 for a typical injected density of about 1.7×10^{18} cm^{-3} and for different QW-widths (8, 10, 12, and 14 nm). The significant influence of the increasing of QW-width is noticeable. This can be explained by the confinement of particles, as shown in Figure 2. One can observe that the gain spectrum has been shifted slightly for the higher wavelength with the increase of the QW-width. The QW-width can improve the gain intensity, but when the concentration of α-Sn is increased, the gain spectrum and the intensity decrease quickly to give a very weak peak, as shown in Figure 3c. To remedy this anomaly, we have inserted a very small quantity of Sn in the barrier with Ge. Figure 3d shows the optical gain of $Ge_{0.99}Sn_{0.01}/Ge_{0.835}Sn_{0.165}/Ge_{0.99}Sn_{0.01}$ QW as a function of photon energy and for different QW-widths (8, 10, 12, and 14 nm). One can observe the significant difference when incorporating the small quantity of the Sn in the barrier. Indeed, the obtained results of the insertion of the α-Sn in the barrier will be helpful the experimental step for the engineering

of $Ge_{1-x}Sn_x/Ge_{1-x}Sn_x/Ge_{1-x}Sn_x$ QWs. Consequentially, it is important to conclude that for the potential fabrication of the $Ge_{1-x}Sn_x/Ge_{1-x}Sn_x/Ge_{1-x}Sn_x$ QWs, the insertion of α-Sn should not exceed 0.155 to ensure high optical gain in mid-infrared emission. In addition, 2×10^{18} cm^{-3} is sufficient to produce gain as an injected carrier density for $Ge_{1-x}Sn_x/Ge_{1-x}Sn_x/Ge_{1-x}Sn_x$ QWs. These sophisticated precision measurements for the α-Sn concentration and injected carrier density are performed in relation to the practice of the 14-band ***k.p*** model; they are not relevant for the 8-band ***k.p*** Hamiltonian. This is due to the second $CB(\Gamma_{8C} - \Gamma_{6C})$ and $VB(\Gamma_{8C} - \Gamma_{8V})$ interaction, which performed the modification noted by the two models.

4. Conclusions

Using 14-band *k.p* Hamiltonian, we have calculated the electron and hole-subband-states and optical gain of $Ge/Ge_{1-x}Sn_x/Ge$ QW for different α-Sn concentrations and QW-widths. Our calculation shows that a 1.5×10^{18} cm^{-3} injection carrier density was sufficient to produce high gain intensity. For the optimization of the α-Sn, our results predicted that $Ge/Ge_{1-x}Sn_x/Ge$ QWs should be realized with a concentration less than 0.155 in device applications involving optical gain in mid-infrared emission at room temperature. Finally, our results indicated that instead of extending the QW-width to enhance the optical gain emission, it is advisable to insert a small quantity of α-Sn into the barrier.

Author Contributions: All authors O.Z., N.M. and S.R. contributed to this work: Conceptualization of this study, Development, Numerical step, Testing, Analysis of results. All authors have read and agreed to the published version of the manuscript.

Funding: The authors declare that no funds, grants, or other support were received during the preparation of this manuscript.

Data Availability Statement: No datasets were generated or analyzed during the current study.

Conflicts of Interest: The authors declare no competing interests.

Appendix A

In our recent paper [18], we have used the 14-band *k.p* Hamiltonian in order to study the VB and CB subband structure and optical emission performance in $Si/Si_yGe_{1-x-y}Sn_x/Si$ Qw materials based on Si indirect band gap and GeSiSn alloys. Thus, taking into account on the structure of GeSn this 14-band model can be adapted to $Ge/Ge_{1-x}Sn_x/Ge$ Qw. However, the 14-band *k.p* Hamiltonian will be presented in $|J, M_J\rangle$ namely Luttinger–Kohn functions bases:

Table A1. Functions bases of Luttinger and Kohn used in atomic notation $|J, M_J\rangle$.

$\left\vert \frac{3}{2}\right\rangle_{\Gamma_{8C}} = \left\vert i\left[-\frac{1}{\sqrt{2}}(X_C + iY_C)\uparrow\right]\right\rangle$	$\left\vert -\frac{3}{2}\right\rangle_{\Gamma_{8C}} = \left\vert i\left[\frac{1}{\sqrt{2}}(X_C - iY_C)\downarrow\right]\right\rangle$
$\left\vert \frac{1}{2}\right\rangle_{\Gamma_{8C}} = \left\vert i\left[\sqrt{\frac{2}{3}}Z_C\uparrow - \frac{1}{\sqrt{6}}(X_C + iY_C)\downarrow\right]\right\rangle$	$\left\vert -\frac{1}{2}\right\rangle_{\Gamma_{8C}} = \left\vert i\left[\sqrt{\frac{2}{3}}Z_C\downarrow + \frac{1}{\sqrt{6}}(X_C - iY_C)\uparrow\right]\right\rangle$
$\left\vert \frac{1}{2}\right\rangle_{\Gamma_{7C}} = \left\vert i\left[\frac{1}{\sqrt{3}}Z_C\uparrow + \frac{1}{\sqrt{3}}(X_C + iY_C)\downarrow\right]\right\rangle$	$\left\vert -\frac{1}{2}\right\rangle_{\Gamma_{7C}} = \left\vert i\left[-\frac{1}{\sqrt{3}}Z_C\downarrow + \frac{1}{\sqrt{3}}(X_C - iY_C)\uparrow\right]\right\rangle$
$\vert+\rangle_{\Gamma_{6C}} = \vert S\uparrow\rangle$	$\vert-\rangle_{\Gamma_{6C}} = \vert S\downarrow\rangle$
$\left\vert \frac{3}{2}\right\rangle_{\Gamma_{8V}} = \left\vert i\left[-\frac{1}{\sqrt{2}}(X + iY)\uparrow\right]\right\rangle$	$\left\vert -\frac{3}{2}\right\rangle_{\Gamma_{8V}} = \left\vert i\left[\frac{1}{\sqrt{2}}(X - iY)\downarrow\right]\right\rangle$
$\left\vert \frac{1}{2}\right\rangle_{\Gamma_{8V}} = \left\vert i\left[\sqrt{\frac{2}{3}}Z\uparrow - \frac{1}{\sqrt{6}}(X + iY)\downarrow\right]\right\rangle$	$\left\vert -\frac{1}{2}\right\rangle_{\Gamma_{8V}} = \left\vert i\left[\sqrt{\frac{2}{3}}Z\downarrow + \frac{1}{\sqrt{6}}(X - iY)\uparrow\right]\right\rangle$
$\left\vert \frac{1}{2}\right\rangle_{\Gamma_{7V}} = \left\vert i\left[\frac{1}{\sqrt{3}}Z\uparrow + \frac{1}{\sqrt{3}}(X + iY)\downarrow\right]\right\rangle$	$\left\vert -\frac{1}{2}\right\rangle_{\Gamma_{7V}} = \left\vert i\left[-\frac{1}{\sqrt{3}}Z\downarrow + \frac{1}{\sqrt{3}}(X - iY)\uparrow\right]\right\rangle$

$$H_{kp}^{14} = \begin{pmatrix}
\left|\frac{3}{2}\right\rangle_{\Gamma_{8C}} & \left|\frac{1}{2}\right\rangle_{\Gamma_{8C}} & \left|\frac{-1}{2}\right\rangle_{\Gamma_{8C}} & \left|\frac{-3}{2}\right\rangle_{\Gamma_{8C}} & \left|\frac{1}{2}\right\rangle_{\Gamma_{7C}} & \left|\frac{-1}{2}\right\rangle_{\Gamma_{7C}} & |+\rangle_{\Gamma_{6C}} & |-\rangle_{\Gamma_{6C}} & \left|\frac{3}{2}\right\rangle_{\Gamma_{8V}} & \left|\frac{1}{2}\right\rangle_{\Gamma_{8V}} & \left|\frac{-1}{2}\right\rangle_{\Gamma_{8V}} & \left|\frac{-3}{2}\right\rangle_{\Gamma_{8V}} & \left|\frac{1}{2}\right\rangle_{\Gamma_{7V}} & \left|\frac{-1}{2}\right\rangle_{\Gamma_{7V}} \\
E_{8c}^{+} & R_c & S_c & 0 & \frac{1}{\sqrt{2}}R_{\Delta c} & \sqrt{2}S_{\Delta c} & -\frac{1}{\sqrt{2}}P'^{-} & 0 & \frac{1}{3}\Delta' & \frac{1}{\sqrt{3}}P_X^{+} & \frac{1}{\sqrt{3}}P_X^{Z} & 0 & \frac{1}{\sqrt{6}}P_X^{+} & \sqrt{\frac{2}{3}}P_X^{Z} \\
cc & E_{8c}^{-} & 0 & S_c & -\sqrt{2}Q_{\Delta c} & -\sqrt{\frac{3}{2}}R_{\Delta c} & \sqrt{\frac{2}{3}}P'^{z} & -\frac{1}{\sqrt{6}}P'^{-} & -\frac{1}{\sqrt{3}}P_X^{-} & \frac{1}{3}\Delta' & 0 & \frac{1}{\sqrt{3}}P_X^{z} & 0 & -\frac{1}{\sqrt{2}}P_X^{+} \\
cc & 0 & E_{8c}^{-} & -R_c & -\sqrt{\frac{3}{2}}R_{\Delta c}^{*} & \sqrt{2}Q_{\Delta c} & \frac{1}{\sqrt{6}}P^{+} & \sqrt{\frac{2}{3}}P'^{z} & -\frac{1}{\sqrt{3}}P_X^{z} & 0 & \frac{1}{3}\Delta' & -\frac{1}{\sqrt{3}}P_X^{+} & \frac{1}{\sqrt{2}}P_X^{-} & 0 \\
0 & cc & cc & E_{8c}^{+} & -\sqrt{2}S_{\Delta c}^{*} & \frac{1}{\sqrt{2}}R_{\Delta c}^{*} & 0 & \frac{1}{\sqrt{2}}P'^{+} & 0 & -\frac{1}{\sqrt{3}}P_X^{z} & \frac{1}{\sqrt{3}}P_X^{-} & \frac{1}{3}\Delta' & \sqrt{\frac{2}{3}}P_X^{z} & -\frac{1}{\sqrt{6}}P_X^{-} \\
cc & cc & cc & cc & E_{7c} & 0 & -\frac{1}{\sqrt{3}}P'^{z} & \frac{1}{\sqrt{3}}P'^{-} & -\frac{1}{\sqrt{6}}P_X^{-} & 0 & -\frac{1}{\sqrt{2}}P_X^{+} & -\sqrt{\frac{2}{3}}P_X^{z} & \frac{-2}{3}\Delta' & 0 \\
cc & cc & cc & cc & 0 & E_{7c} & \frac{1}{\sqrt{3}}P'^{+} & -\frac{1}{\sqrt{3}}P'^{z} & -\sqrt{\frac{2}{3}}P_X^{z} & \frac{1}{\sqrt{2}}P_X^{-} & 0 & \frac{1}{\sqrt{6}}P_X^{+} & 0 & \frac{-2}{3}\Delta' \\
cc & cc & cc & 0 & cc & cc & E_6 & 0 & -\frac{1}{\sqrt{2}}P^{+} & \sqrt{\frac{2}{3}}P^{z} & \frac{1}{\sqrt{6}}P^{-} & 0 & \frac{1}{\sqrt{3}}P^{z} & \frac{1}{\sqrt{3}}P^{-} \\
0 & cc & cc & cc & cc & cc & 0 & E_6 & 0 & -\frac{1}{\sqrt{6}}P^{+} & \sqrt{\frac{2}{3}}P^{z} & \frac{1}{\sqrt{2}}P^{z} & \frac{1}{\sqrt{3}}P^{+} & -\frac{1}{\sqrt{3}}P^{z} \\
cc & cc & cc & 0 & cc & cc & cc & 0 & E_8^{+} & R & S & 0 & \frac{1}{\sqrt{2}}R_{\Delta} & \sqrt{2}S_{\Delta} \\
cc & cc & 0 & cc & 0 & cc & cc & cc & cc & E_8^{-} & 0 & S & -\sqrt{2}Q_{\Delta} & \sqrt{\frac{2}{3}}R_{\Delta} \\
cc & 0 & cc & cc & cc & 0 & cc & cc & cc & 0 & E_8^{-} & -R & -\sqrt{\frac{3}{2}}R_{\Delta}^{*} & \sqrt{2}Q_{\Delta} \\
0 & cc & cc & cc & cc & cc & 0 & cc & 0 & cc & cc & E_8^{+} & -\sqrt{2}S_{\Delta} & \frac{1}{\sqrt{2}}R_{\Delta} \\
cc & 0 & cc & cc & cc & 0 & cc & cc & cc & cc & cc & cc & E_7 & 0 \\
cc & cc & 0 & cc & 0 & cc & cc & cc & cc & cc & cc & cc & 0 & E_7
\end{pmatrix} \quad \text{(A1)}$$

where,

$$E_{8C}^{\pm} = E_G + E_{GC} + \Delta_C - \frac{(\Delta'/3)^2}{E_G + E_{GC} + \Delta_C} - \widetilde{\gamma}_{C1}\widetilde{k}^2 \pm Q_C \quad \text{(A2)}$$

$$E_{7C} = E_G + E_{GC} - \frac{(2\Delta'/3)^2}{E_G + E_{GC} + \Delta} - \widetilde{\gamma}_{\Delta C1}\widetilde{k}^2 \quad \text{(A3)}$$

$$E_8^{\pm} = \frac{(\Delta'/3)^2}{E_G + E_{GC} + \Delta_C} - \widetilde{\gamma}_1\widetilde{k}^2 \pm Q \quad \text{(A4)}$$

$$E_7 = \frac{(2\Delta'/3)^2}{E_G + E_{GC} + \Delta} - \Delta - \widetilde{\gamma}_{\Delta 1}\widetilde{k}^2 \quad \text{(A5)}$$

$$E_6 = \breve{\gamma}_C \breve{k}^2 + E_G \quad \text{(A6)}$$

$$R_C = 2\sqrt{3}\widetilde{\gamma}_{C3}\widetilde{k}_z\widetilde{k}_-,\ S_C = \sqrt{3}\left[\widetilde{\gamma}_{C2}\left(\widetilde{k}_x^2 - \widetilde{k}_y^2\right) - 2i\widetilde{\gamma}_{C3}\widetilde{k}_x\widetilde{k}_y\right],\ Q_C = \widetilde{\gamma}_{C2}\left(2\widetilde{k}_z^2 - \widetilde{k}_\rho^2\right) \quad \text{(A7)}$$

$$R_{\Delta C} = 2\sqrt{3}\widetilde{\gamma}_{\Delta C3}\widetilde{k}_z\widetilde{k}_-,\ S_{\Delta C} = \sqrt{3}\left[\widetilde{\gamma}_{\Delta C2}\left(\widetilde{k}_x^2 - \widetilde{k}_y^2\right) - 2i\widetilde{\gamma}_{\Delta C3}\widetilde{k}_x\widetilde{k}_y\right],\ Q_{\Delta C} = \widetilde{\gamma}_{\Delta C2}\left(2\widetilde{k}_z^2 - \widetilde{k}_\rho^2\right) \quad \text{(A8)}$$

$$E_6 = E_G + \widetilde{\gamma}_C\widetilde{k}^2,\ E_8^{\pm} = -\widetilde{\gamma}_1\widetilde{k}^2 \pm Q,\ E_7 = -\Delta - \widetilde{\gamma}_{\Delta 1}\widetilde{k}^2 \quad \text{(A9)}$$

$$R = 2\sqrt{3}\widetilde{\gamma}_3\widetilde{k}_z\widetilde{k}_-,\ S = \sqrt{3}\left[\widetilde{\gamma}_2\left(\widetilde{k}_x^2 - \widetilde{k}_y^2\right) - 2i\widetilde{\gamma}_3\widetilde{k}_x\widetilde{k}_y\right],\ Q = \widetilde{\gamma}_2\left(2\widetilde{k}_z^2 - \widetilde{k}_\rho^2\right) \quad \text{(A10)}$$

$$R_\Delta = 2\sqrt{3}\widetilde{\gamma}_{\Delta 3}\widetilde{k}_z\widetilde{k}_-,\ S_\Delta = \sqrt{3}\left[\widetilde{\gamma}_{\Delta 2}\left(\widetilde{k}_x^2 - \widetilde{k}_y^2\right) - 2i\widetilde{\gamma}_{\Delta 3}\widetilde{k}_x\widetilde{k}_y\right],\ Q_\Delta = \widetilde{\gamma}_{\Delta 2}\left(2\widetilde{k}_z^2 - \widetilde{k}_\rho^2\right) \quad \text{(A11)}$$

The matrix elements (P_X, P' and P) are given by:

$$P_X = \frac{\hbar}{m_0}\langle X_C|p_z|iY\rangle = -\frac{\hbar}{m_0}\langle Y|p_z|iX_C\rangle,\ P' = \frac{\hbar}{m_0}\langle S|p_x|iX_C\rangle,\ P = \frac{\hbar}{m_0}\langle S|p_x|iX\rangle \quad \text{(A12)}$$

where S, (X, Y), X_C represent the wave functions which appertain respectively to $\{\Gamma_{6c}\}$, $\{\Gamma_{8C}, \Gamma_{7C}\}$ and $\{\Gamma_{8v}, \Gamma_{7v}\}$. Note that the matrix elements (P_X, P' and P) are real and their corresponding energies are:

$$E_P = \frac{2m_0}{\hbar}P^2\ ;\ E_{PX} = \frac{2m_0}{\hbar}P_X^2\ ;\ E'_P = \frac{2m_0}{\hbar}P'^2 \quad \text{(A13)}$$

We notice that in our calculation the momentum matrix elements have been deduced through the band structure of the bulk Ge and α-Sn then we have used linear interpolation for GeSn QWs based on work given by S. L. Chuang [21].

The spin-orbit splitting energies are given as:

$$\begin{aligned}\Delta &= \tfrac{3\hbar}{4m_0^2c^2}\langle iX|\left[\vec{\nabla}U\wedge\vec{p}\right]_y|Z\rangle\\ \Delta_C &= \tfrac{3\hbar}{4m_0^2c^2}\langle iX_C|\left[\vec{\nabla}U\wedge\vec{p}\right]_y|Z\rangle\\ \Delta' &= \tfrac{3\hbar}{4m_0^2c^2}\langle iX_C|\left[\vec{\nabla}U\wedge\vec{p}\right]_y|Z\rangle\end{aligned} \tag{A14}$$

The adapted Luttinger parameters of the second CB $\{\Gamma_{8C},\Gamma_{7C}\}$ are given by:

$$\widetilde{\gamma}_{C1} = \gamma_{C1} + \frac{1}{3}\left[\frac{E'_P}{E_{GC}+\Delta_C}\right] + \frac{E_{PX}}{3}\left[\frac{1}{E_G+E_{GC}+\Delta_C} + \frac{1}{\Delta+E_G+E_{GC}+\Delta_C}\right] \tag{A15}$$

$$\widetilde{\gamma}_{C2} = \gamma_{C2} + \frac{1}{6}\left[\frac{E'_P}{E_{GC}+\Delta_C}\right] - \frac{1}{6}\left[\frac{1}{\Delta+E_G+E_{GC}+\Delta_C}\right] \tag{A16}$$

$$\widetilde{\gamma}_{C3} = \gamma_{C3} + \frac{1}{6}\left[\frac{E'_P}{E_{GC}+\Delta_C}\right] + \frac{1}{6}\left[\frac{1}{\Delta+E_G+E_{GC}+\Delta_C}\right] \tag{A17}$$

$$\widetilde{\gamma}_{\Delta C1} = \gamma_{C1} + \frac{1}{3}\left[\frac{E'_P}{E_{GC}+\Delta_C}\right] + \frac{E_{PX}}{3}\left[\frac{1}{E_G+E_{GC}+\Delta_C} + \frac{1}{\Delta+E_G+E_{GC}+\Delta_C} - \frac{2}{E_G+E_{GC}}\right] \tag{A18}$$

$$\widetilde{\gamma}_{\Delta C2} = \gamma_{C2} + \frac{1}{6}\left[\frac{E'_P}{E_{GC}+\Delta_C}\right] + \frac{E_{PX}}{12}\left[\frac{2}{E_G+E_{GC}+\Delta_C} - \frac{1}{\Delta+E_G+E_{GC}+\Delta_C} - \frac{1}{E_G+E_{GC}}\right] \tag{A19}$$

$$\widetilde{\gamma}_{\Delta C3} = \gamma_{C3} + \frac{1}{6}\left[\frac{E'_P}{E_{GC}+\Delta_C}\right] - \frac{E_{PX}}{12}\left[\frac{2}{E_G+E_{GC}+\Delta_C} - \frac{1}{\Delta+E_G+E_{GC}+\Delta_C} - \frac{1}{E_G+E_{GC}}\right] \tag{A20}$$

The adapted Luttinger parameter of the first CB $\{\Gamma_{6C}\}$ is given by:

$$\widetilde{\gamma}_C = \gamma_C - \frac{E_{PX}}{3}\left[\frac{2}{E_G} + \frac{1}{E_G+\Delta}\right] + \frac{E'_P}{3}\left[\frac{2}{E_G+\Delta_C} + \frac{1}{E_{GC}}\right] \tag{A21}$$

The adapted Luttinger parameters of the top VB $\{\Gamma_{8v},\Gamma_{7v}\}$ are given by:

$$\widetilde{\gamma}_1 = \gamma_1 - \frac{E_P}{3E_G} - \frac{E_{PX}}{3}\left[\frac{1}{E_G+E_{GC}} + \frac{1}{\Delta+E_G+E_{GC}+\Delta_C}\right] \tag{A22}$$

$$\widetilde{\gamma}_2 = \gamma_2 - \frac{E_P}{6E_G} + \frac{1}{6}\left[\frac{E_{PX}}{E_G+E_{GC}}\right] \tag{A23}$$

$$\widetilde{\gamma}_3 = \gamma_3 - \frac{E_P}{6E_G} - \frac{1}{6}\left[\frac{E_{PX}}{E_G+E_{GC}}\right] \tag{A24}$$

$$\widetilde{\gamma}_{\Delta 1} = \gamma_1 - \frac{E_P}{3E_G} - \frac{E_{PX}}{3}\left[\frac{1}{E_G+E_{GC}} + \frac{1}{E_G+E_{GC}+\Delta_C} - \frac{2}{\Delta+E_G+E_{GC}+\Delta_C}\right] \tag{A25}$$

$$\widetilde{\gamma}_{\Delta 2} = \gamma_2 - \frac{E_P}{6E_G} + \frac{E_{PX}}{12}\left[\frac{2}{E_G+E_{GC}} - \frac{1}{E_G+E_{GC}+\Delta_C} - \frac{1}{\Delta+E_G+E_{GC}+\Delta_C}\right] \tag{A26}$$

$$\widetilde{\gamma}_{\Delta 3} = \gamma_2 - \frac{E_P}{6E_G} - \frac{E_{PX}}{12}\left[\frac{2}{E_G+E_{GC}} - \frac{1}{E_G+E_{GC}+\Delta_C} - \frac{1}{\Delta+E_G+E_{GC}+\Delta_C}\right] \tag{A27}$$

It is important to note that in H_{kp} matrix the parameters P'^z, P'^+, P'^- and Δ' are equal to zero for *Oh*-symmetry groups such as IV–IV semiconductors Si, Ge, α-Sn and are nonnull for *Td*-symmetry groups such as III–V or II–VI.

References

1. Marzban, B.; Stange, D.; Rainko, D.; Ikonic, Z.; Buca, D.; Witzens, J. Modeling of a SiGeSn quantum well laser. *Photonics Res.* **2021**, *9*, 1234. [CrossRef]
2. Deales, T.; Marko, I.P.; Schulz, S.; O'Halloran, E.; Ghetmiri, S.; Du, W.; Zhou, Y.; Yu, S.-Q.; Margetis, J.; Tolle, J.; et al. $Ge_{1-x}Sn_x$ alloys: Consequences of band mixing effects for the evolution of the band gap Γ-character with Sn concentration. *Sci. Rep.* **2019**, *9*, 14077. [CrossRef]
3. Losert, P.M.; Eriksson, M.A.; Joynt, R.; Rahman, R.; Scappucci, G.; Coppersmith, S.N.; Friesen, M. Practical strategies for enhancing the valley splitting in Si/SiGe quantum wells. *Phys. Rev. B* **2023**, *108*, 125405. [CrossRef]
4. Junkin, T.M.; Harpt, B.; Feng, Y.; Losert, M.P.; Rahman, R.; Dodson, J.P.; Wolfe, M.A.; Savage, D.E.; Lagally, M.G.; Coppersmith, S.N.; et al. SiGe quantum wells with oscillating Ge concentrations for quantum dot qubits. *Nat. Commun.* **2022**, *13*, 7777. [CrossRef] [PubMed]
5. Ridene, S.; Boujdaria, K.; Bouchriha, H.; Fishman, G. Infrared absorption in $Si/Si_{1-x}Ge_x/Si$ quantum wells. *Phys. Rev. B* **2001**, *64*, 085329. [CrossRef]
6. Rainko, D.; Ikonic, Z.; Vukmirović, N.; Stange, D.; Driesch, N.V.-D.; Grützmacher, D.; Buca, D. Investigation of carrier confinement in direct bandgap GeSn/SiGeSn 2D and 0D heterostructures. *Sci. Rep.* **2018**, *8*, 15557. [CrossRef]
7. Mączko, H.S.; Kudrawiec, R.; Gladysiewicz, M. Strain engineering of transverse electric and transverse magnetic mode of material gain in GeSn/SiGeSn quantum wells. *Sci. Rep.* **2019**, *9*, 3316. [CrossRef] [PubMed]
8. Jernigan, G.G.; Mahadik, N.A.; Twigg, M.E.; Jackson, E.M.; Nolde, J.A. SiGeSn buffer layer for the growth of GeSn films. *J. Appl. Phys.* **2023**, *134*, 025305. [CrossRef]
9. Zaima, S.; Nakatsuka, O.; Taoka, N.; Kurosawa, M.; Takeuchi, W.; Sakashita, M. Growth and applications of GeSn-related group-IV semiconductor materials. *Sci. Technol. Adv. Mater.* **2015**, *16*, 043502. [CrossRef] [PubMed]
10. Wang, B.; Michael, R.H.; Harris, T.R.; Wallace, P.M.; Kouvetakis, K. Enhanced optical and electrical performance of $Ge_{1-x}Sn_x/Ge/Si(100)$ (x = 0.062) semiconductor via inductively coupled H_2 plasma treatments. *Semicond. Sci. Technol.* **2019**, *34*, 045014. [CrossRef]
11. Ghosh, S.; Mukhopadhyay, B.; Sen, G.; Basu, P.K. Performance analysis of GeSn/SiGeSn quantum well infrared photodetector in terahertz wavelength region. *Phys. E* **2020**, *115*, 113692. [CrossRef]
12. Ghosh, S.; Bhattacharyya, A.; Sen, G.; Mukhopadhyay, B. Optimization of different structural parameters of GeSn/SiGeSn Quantum Well Infrared Photodetectors (QWIPs) for low dark current and high responsivity. *J. Comput. Electron.* **2021**, *20*, 1224–1233. [CrossRef]
13. Xu, C.; Jiang, L.; Kouvetakis, J.; Menéndez, J. Optical properties of $Ge_{1-x-y}Si_xSn_y$ alloys with y > x: Direct bandgaps beyond 1550 nm. *Appl. Phys. Lett.* **2013**, *103*, 072111. [CrossRef]
14. Yamaha, T.; Shibayama, S.; Asano, T.; Kato, K.; Sakashita, M.; Takeuchi, W.; Nakatsuka, O.; Zaima, S. Experimental observation of type-I energy band alignment in lattice-matched $Ge_{1-x-y}Si_xSn_y/Ge$ heterostructures. *Appl. Phys. Lett.* **2016**, *108*, 061909. [CrossRef]
15. Wirths, S.; Geiger, R.; von den Driesch, N.; Mussler, G.; Stoica, T.; Mantl, S.; Ikonic, Z.; Luysberg, M.; Chiussi, S.; Hartmann, J.M.; et al. Lasing in direct-bandgap GeSn alloy grown on Si. *Nat. Photonics* **2015**, *9*, 88. [CrossRef]
16. Fujisawa, T.; Arai, M.; Saitoh, K. Microscopic gain analysis of modulation doped GeSn/SiGeSn quantum wells: Epitaxial design toward high-temperature lasing. *Opt. Express* **2019**, *27*, 2457. [CrossRef]
17. Lin, P.-H.; Ghosh, S.; Chang, G.-E. Theoretical Analysis of GeSn Quantum Dots for Photodetection Applications. *Sensors* **2024**, *24*, 1263. [CrossRef] [PubMed]
18. Zitouni, O.; Saidi, H.; Ridene, S. Investigation of α-Sn Dependence of Band Structure and Optical Emission in $Si/Si_yGe_{1-x-y}Sn_x/Si$ Quantum Well Laser. *Silicon* **2024**, *16*, 3573–3581. [CrossRef]
19. Asada, M.; Kameyama, A.; Suematsu, Y. Gain and intervalence band absorption in quantum-well lasers. *IEEE J. Quantum Electron.* **1984**, *20*, 745–753. [CrossRef]
20. Chen, Z.; Ikonic, Z.; Indjin, D.; Kelsall, R.W. Design optimization of tensile-strained SiGeSn/GeSn quantum wells at room temperature. *J. Appl. Phys.* **2021**, *129*, 123102. [CrossRef]
21. Chuang, S.L. *Physics of Photonic Devices*, 2nd ed.; Wiley: New York, NY, USA, 2009.

Disclaimer/Publisher's Note: The statements, opinions and data contained in all publications are solely those of the individual author(s) and contributor(s) and not of MDPI and/or the editor(s). MDPI and/or the editor(s) disclaim responsibility for any injury to people or property resulting from any ideas, methods, instructions or products referred to in the content.